

# Segment Anything in 3D Gaussians

Xu Hu<sup>1,2</sup> Yuxi Wang<sup>2,3</sup> Lue Fan<sup>3,4</sup> Junsong Fan<sup>2,3</sup> Junran Peng<sup>3,5</sup>  
 Zhen Lei<sup>2,3,4</sup> Qing Li<sup>1\*</sup> Zhaoxiang Zhang<sup>2,3,4\*</sup>

<sup>1</sup>The Hong Kong Polytechnic University

<sup>2</sup>Center for Artificial Intelligence and Robotics, HKISI, CAS

<sup>3</sup>Institute of Automation, Chinese Academy of Sciences

<sup>4</sup>University of Chinese Academy of Sciences <sup>5</sup>Chongyue Technology

xu0529.hu@connect.polyu.hk, {yuxiwang93, jrpeng4ever}@gmail.com,

{fanlue2019, junsong.fan, zhaoxiang.zhang}@ia.ac.cn, zlei@nlpr.ia.ac.cn, csqli@comp.polyu.edu.hk

## Abstract

*3D Gaussian Splatting has emerged as an alternative 3D representation of Neural Radiance Fields (NeRFs), benefiting from its high-quality rendering results and real-time rendering speed. Considering the 3D Gaussian representation remains unparsed, it is necessary first to execute object segmentation within this domain. Subsequently, scene editing and collision detection can be performed, proving vital to a multitude of applications, such as virtual reality (VR), augmented reality (AR), game/movie production, etc. In this paper, we propose a novel approach to achieve object segmentation in 3D Gaussian via an interactive procedure without any training process and learned parameters. We refer to the proposed method as SA-GS, for Segment Anything in 3D Gaussians. Given a set of clicked points in a single input view, SA-GS can generalize SAM to achieve 3D consistent segmentation via the proposed multi-view mask generation and view-wise label assignment methods. We also propose a cross-view label-voting approach to assign labels from different views. In addition, in order to address the boundary roughness issue of segmented objects resulting from the non-negligible spatial sizes of 3D Gaussian located at the boundary, SA-GS incorporates the simple but effective Gaussian Decomposition scheme. Extensive experiments demonstrate that SA-GS achieves high-quality 3D segmentation results, which can also be easily applied for scene editing and collision detection tasks. Codes will be released soon.*

## 1. Introduction

3D scene understanding is a challenging and crucial task in computer vision and computer graphics, which involves scene reconstruction from images or videos and the perception of a given 3D real-world environment. Researchers

have conducted extensive studies in scene reconstruction and 3D scene perception in recent years. For instance, Neural Radiance Fields (NeRF) [4, 10, 20, 28] have significantly contributed to the progress of 3D scene reconstruction by representing scenes in an implicit way. In the field of scene perception, continuous research is being conducted on 3D detection and semantic segmentation, based on the representation of range images [6, 18], point clouds [7, 9, 14, 24, 27], and Bird’s Eye View (BEV) [15, 22, 23, 25, 31]. Although current methods have attained noteworthy success in 3D scene understanding, the time-consuming nature of NeRF and the high costs associated with 3D data collection pose challenges for scaling up these approaches.

Alternatively, SA3D [3] addresses the aforementioned challenges by enhancing the 2D foundational model (*i.e.* SAM [13]) with 3D perception through the incorporation of a 3D representation model. SA3D demonstrates notable success by leveraging NeRF to generate 2D views and aligning 2D segmentation results with the 3D scene. However, the substantial training and rendering time costs associated with NeRF make it impractical for large-scale 3D scenes. Consequently, in this work, we focus on 3D Gaussian Splatting (3D-GS) [11] as a prospective method for modeling static 3D scenes. 3D-GS characterizes intricate scenes by employing numerous colored 3D Gaussians, rendering them into camera views through splatting-based rasterization. Through differentiable rendering and gradient-based optimization, the positions, sizes, rotations, colors, and opacities of these Gaussians can be finely tuned to accurately represent the 3D scene, availing for the comprehension of a 3D environment.

Benefiting from the properties of high-quality and real-time rendering in 3D-GS, it is impressive to use these explicit representations to capture the shape and appearance of complex objects. Specifically, based on the 3D Gaussian volume, we can effectively achieve scene perception

\*Corresponding author

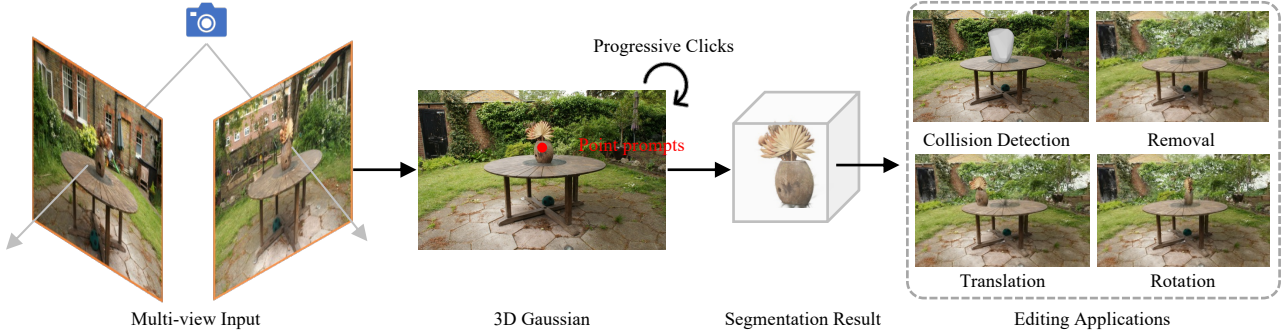


Figure 1. We propose an effective 3D object segmentation method in 3D Gaussian without any training process. The segmented mask contributes to the realization of various applications, including collision detection, translation, rotation and removal, etc.

via equipping the 2D foundation model as SA3D [3] statement. Different from SA3D leveraging implicit NeRF as a 3D prior to connecting multiple 2D views, our method (**SA-GS**) applies effect and explicit 3D-GS representation to perform 3D object segmentation. Subsequently, scene editing and collision detection can be executed readily, as shown in Figure 1, which is essential to various applications, such as virtual reality(VR), augmented reality(AR), and games/movie production. Moreover, in contrast to the existing labor-intensive data collection perception frameworks that require point or multi-view images, 3D-GS offers a source of high-quality training data without the need for extensive manual efforts. This aspect holds significant promise for future research endeavors.

In this paper, we propose a novel approach to achieve object segmentation in 3D Gaussian via an interactive procedure without any training process and learned parameters. Specifically, by leveraging the 2D foundational model SAM [13], SA-GS can generate a segmented mask from a single input view based on the given point prompts. Starting from the obtained mask, we automatically generate multi-view masks and achieve consistent 3D segmentation via the proposed view-wise label assignment. In addition, to address the boundary roughness issue of segmented objects resulting from the non-negligible spatial sizes of 3D Gaussian located at the boundary, SA-GS incorporates the simple but effective Gaussian Decomposition scheme. Moreover, our segmented 3D Gaussians can be seamlessly employed in collision detection and scene editing tasks, like removal, translation, rotation, etc. In summary, the contributions of this paper are as follows.

- We propose a simple yet effective method for object segmentation in 3D Gaussians without any training process and learnable parameters.
- Efficient collision detection and scene editing, such as object removal, translation, and rotation within 3D scenes, can be performed readily based on the segmentation of SA-GS.
- We conduct extensive segmentation experiments on a

considerable amount of 3D scenes, demonstrating the effectiveness of our proposed method.

## 2. Related Work

### 2.1. 3D Gaussian Splitting

3D Gaussian Splatting [11] is a technique for scene reconstruction, which has been shown to be an alternative 3D representation as NeRF, benefiting from both its high-quality rendering results and real-time rendering speed. Recent research on this technique contains applying 3D Gaussian in dynamic scene and combining it with diffusion model to achieve 3D generation. Dynamic 3D Gaussians [17] extends Gaussian Splatting to dynamic scenes via tracking 3D objects modeled as a set of 3D Gaussians. DreamGaussian [29], GaussianDreamer [32] and GSGEN [5] combine 3D Gaussians with diffusion models to generate high-quality 3D assets. In this work, we for the first time lift 2D foundation model-SAM[13] to 3D Gaussians in order to achieve 3D object segmentation in this Gaussian space.

### 2.2. Segmentation in NeRFs

Neural Radiance Fields (NeRFs) are a popular way of representing 3D scenes implicitly with neural networks. Many researchers have explored how to segment objects in 3D using NeRFs, for various applications such as novel view synthesis, semantic segmentation, 3D inpainting, and language grounding. Some methods, such as Semantic-NeRF [33], NVOS [26], and SA3D [3], use different types of inputs to guide the segmentation, such as semantic labels, user scribbles, or 2D masks. Other methods, such as N3F [30], DFF [30], LERF [12], and ISRF [8], learn additional feature fields that are aligned with NeRFs, and use 2D visual features from pre-trained models or language embeddings to query the 3D features. These methods usually require modifying or retraining the original NeRF models or training other specific parameters to obtain the 3D segmentation. However, limited by the representation and rendering speed of NeRF, it is challenging to apply it to more prac-

tical applications, such as scene editing, collision analysis, etc. Benefiting from the purely explicit representation of 3D Gaussian, we can directly achieve 3D segmentation via an interactive way without any learned parameters and training process, and can apply for many other applications.

### 3. Method

In this section, we first present the preliminary in 3D Gaussian Splatting in Sec. 3.1 for clear understanding. We then define the problem and task in Sec. 3.2. Sec. 3.3, Sec. 3.4 and Sec. 3.5 elaborate on the technical details.

#### 3.1. Preliminary: 3D Gaussian Splatting

3D Gaussian Splatting (3D GS) [11] is an emerging method for real-time radiance field rendering. It has been proven effective in Novel View Synthesis with high rendering quality as NeRF and real-time rendering speed. 3D GS represents scenes with a set of 3D Gaussians. Specifically, each 3D Gaussian is parameterized by a position  $\mu \in \mathbb{R}^3$ , a covariance matrix  $\Sigma$ , an opacity value  $\alpha$ , and spherical harmonics (SH).

To render an image, it uses the splatting rendering pipeline, where 3D Gaussians are projected onto the 2D image plane. The projection transforms 3D Gaussians into 2D Gaussians in the image plane. All 2D Gaussians are blended together by the  $\alpha$ -blending algorithm to generate the color:

$$\mathbf{c} = \sum_{i \in N} \mathbf{c}_i \alpha_i \prod_{j=1}^{i-1} (1 - \alpha_j), \quad (1)$$

During the  $\alpha$ -blending process, for each 2D Gaussian, only the 2D points with probability density larger than a certain threshold are calculated. This means a 2D Gaussian and 3D Gaussian can be intuitively regarded as a 2D **ellipse** and a 3D **ellipsoid** respectively. Empirically, for an axis of the ellipse, its length is set to  $3\sigma$ , where  $\sigma$  is the square root of the variance in the axis.

#### 3.2. Problem Definition

Given a set of trained 3D gaussians  $\mathbb{G} = \{\mathbf{g}_0, \mathbf{g}_1, \dots, \mathbf{g}_n\}$  and a random initial view  $\mathbf{v}_0$ , users could offer 2D point prompt set  $\mathbb{P}_{2D} = \{\mathbf{p}_0, \mathbf{p}_1, \dots, \mathbf{p}_m\}$  to specify a 2D object in view  $\mathbf{v}_0$ . Our algorithm is supposed to segment the corresponding 3D object  $\mathbb{O}$  in  $\mathbb{G}$  according to the human prompts, where  $\mathbb{O}$  is a subset of  $\mathbb{G}$ .

Let  $\mathbf{m}_i$  denote the projected binary mask of  $\mathbb{O}$  in  $i$ -th view, an accurate segmentation  $\mathbb{O}$  means  $\mathbf{m}_i$  equals to  $\mathbf{m}_i^*$  for  $\forall i \in \{0, 1, \dots, n\}$ . Here  $\mathbf{m}_i^*$  is the ground truth mask of  $\mathbb{O}$  in  $i$ -th view. Different from the conventional 2D segmentation mask in the image or 3D segmentation task in the point cloud, there is no ground truth for 3D Gaussians. Thus, our algorithm is designed to minimize the difference between  $\mathbf{m}_i$  and  $\mathbf{m}_i^*$ .

#### 3.3. Segment 3D Gaussians with 2D Mask

**3D Prompts for Multiview Masks Generation** By the definition in Sec. 3.2, users are given the first rendered view to specify the target object. However, only the first view is far from sufficient to segment the target object in 3D space. So here we first generate multiview masks to aid the 3D segmentation. With multiple masks from different views, a 3D object can be segmented by the intersection of the corresponding frustum of these masks.

The core of obtaining masks is to generate 2D prompt points in each view. Denoting the  $i$ -th 2D prompt point in the first given view  $\mathbf{v}_0$  as  $\mathbf{p}_i^0$ , we define the corresponding 3D prompt  $\mathbf{p}_i^{3D}$  as:

$$\arg \min_{\mu} \{d(\mu), d(\mu) > 0 \mid \mu \in \mathbb{G}, \|\mathbf{P}_0 \mu - \mathbf{p}_i^0\|_1 < \epsilon\}, \quad (2)$$

where  $d(\mu)$  is the depth of Gaussian center  $\mu$  and  $\mathbf{P}_0$  is the projection for initial view  $\mathbf{v}_0$ . Thus  $\mathbf{P}_0 \mu$  is the position of  $\mu$  in view  $\mathbf{v}_0$ . Eq. 2 indicates that the corresponding 3D prompt of  $\mathbf{p}_i$  is the center of a certain 3D Gaussian. This center meets two requirements: (1) it has a similar projected position with  $\mathbf{p}_i$  with a Manhattan distance less than  $\epsilon$ , and (2) if there are multiple 3D Gaussian centers satisfying the first requirement, the one with the smallest positive depth is selected as the 3D prompt.

For all the 2D prompt points in the first view, we could get a set of 3D prompt by Eq. 2. Then for another view  $\mathbf{v}_i$ , we project these 3D prompts into the 2D plane, resulting in 2D prompts in the view  $\mathbf{v}_i$ . In this way, we obtain 2D prompts in all views, and all masks are obtained by prompting the SAM.

**View-wise Label Assignment** With all the masks, we proceed to assign binary labels to each 3D Gaussian. In particular, we maintain a matrix  $\mathbf{L}$ , whose element  $\mathbf{L}_{ij}$  is defined by

$$\mathbf{L}_{ij} = \begin{cases} 1 & \text{if } \mathbf{P}_j \mu_i \in \mathbf{m}_j, \\ 0 & \text{if } \mathbf{P}_j \mu_i \notin \mathbf{m}_j, \end{cases} \quad (3)$$

where  $\mu_i$  is the  $i$ -th Gaussian center of the scene and  $\mathbf{m}_j$  is the foreground mask in  $j$ -th view.  $\mathbf{P}_j$  stands for the projection matrix of  $j$ -th view.

#### 3.4. Gaussian Decomposition

Eq. 3 assign labels to 3D Gaussians only by the projected position of its center. However, 3D Gaussian has non-negligible spatial volume, so those Gaussians projected to the mask boundary usually have a part out of the boundary, greatly increasing the roughness of boundaries. A straightforward solution is directly removing the Gaussians across mask boundaries. However, such a solution greatly damages the 3D structures of the object.

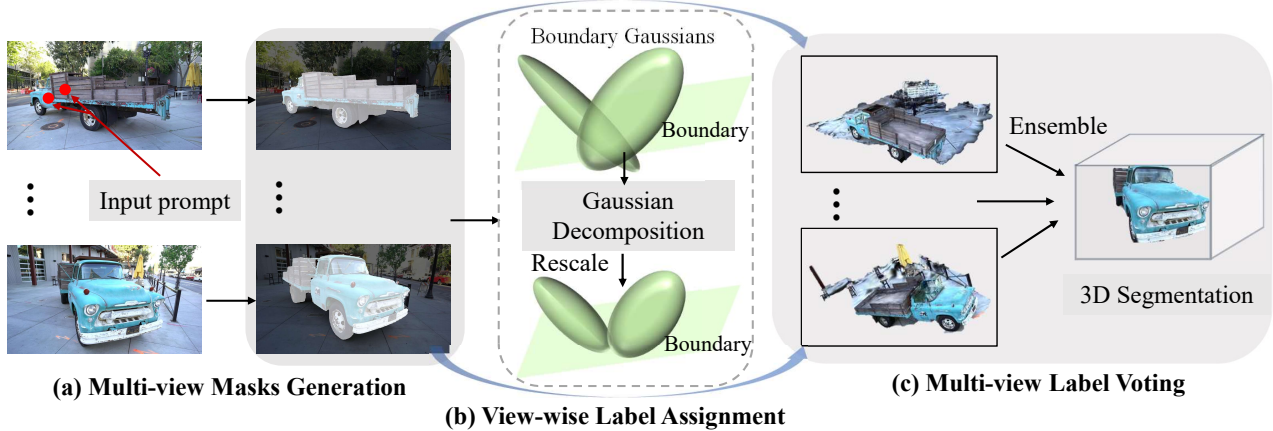


Figure 2. Pipeline of our proposed SA-GS. (a) Given a set of clicked points on the 1<sup>st</sup> rendered view, we utilize SAM to generate masks for corresponding objects under every view automatically; (b) For every view, Gaussian Decomposition is first performed to address the issue of boundary roughness and then label propagation is implemented to assign binary labels to each 3D Gaussian; (c) Finally, with assigned 3D labels from all views, we adopt a simple yet effective voting strategy to determine the segmented Gaussians.

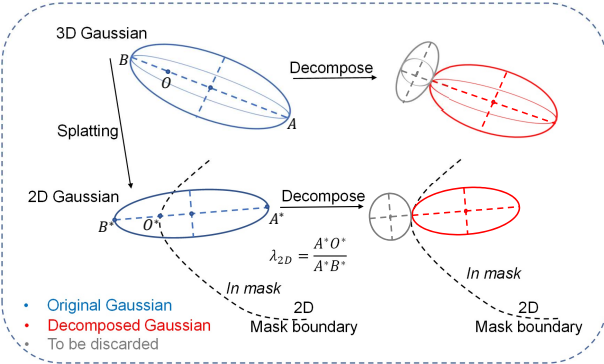


Figure 3. Illustration of the Gaussian Decomposition process.

To address this issue, we propose the *Gaussian Decomposition* to mitigate the boundary roughness while maintaining the 3D structures as complete as possible. Figure. 3 illustrates the basic idea of Gaussian decomposition. It has two basic steps to achieve the Gaussian decomposition: (1) For each 3D Gaussian, we obtain the corresponding 2D Gaussian by projection and mark it as a boundary Gaussian if one of its long-axis endpoints is outside of the 2D mask. Then, as shown in Figure. 3 we denote the two ends of the long axis of a 2D Gaussian as  $A^*$  and  $B^*$ , and the intersection of  $A^*B^*$  and mask boundary is  $O^*$ .  $A$ ,  $B$ , and  $O$  are the corresponding 3D points in the long axis of the 3D Gaussian. Assuming  $A^*$  is in the mask while  $B^*$  is out of the mask, we define

$$\lambda_{3D} = \frac{OA}{AB}, \quad (4)$$

$$\lambda_{2D} = \frac{O^*A^*}{A^*B^*}. \quad (5)$$

(2) After obtaining the boundary Gaussians, we solve the ratio  $\lambda_{3D}$  by first calculating  $\lambda_{2D}$  and then decompose the

original 3D Gaussian according to  $\lambda_{3D}$ .

However, the transformation from  $\lambda_{2D}$  to  $\lambda_{3D}$  is not straightforward because the perspective projection from 3D space to 2D space is not affine, which means the ratios are different. Fortunately, 3D Gaussian Splatting leverages local affine approximation to simplify the rendering process. It projects 3D Gaussian to the 2D plane by

$$\Sigma' = JW\Sigma W^T J^T \quad (6)$$

where  $\Sigma$ ,  $\Sigma'$  are the covariance matrix of the 3D and 2D gaussian distribution, respectively.  $W$  is the projection transformation and  $J$  is the Jacobian of affine approximation derived in EWA algorithm [34]. Eq. 6 indicates that Gaussian Splatting simplifies the perspective projection to an affine projection, thus decomposition scaling ratio  $\lambda_{3D}$  in 3D space is equivalent to the ratio  $\lambda_{2D}$  in the 2D plane.

Let  $g$  denote a 3D Gaussian across the boundary. Its scale in long axis and the 3D center are defined as  $s$  and  $\mu$ , respectively. We have

$$s' = \lambda_{2D}s, \quad (7)$$

$$\mu' = \mu + \frac{1}{2}(s - \lambda_{2D}s)\mathbf{e}, \quad (8)$$

where  $\mathbf{e}$  is the unit vector pointing from the 3D Gaussian center to the in-mask endpoint of the long axis. The decomposed Gaussian  $g'$  adopt  $\mu'$  and  $s'$  as the new center and long-axis scale, maintaining other properties unchanged. Another decomposed Gaussian outside of the mask is removed.

### 3.5. Multiview Label Voting

So far, every 3D Gaussian including the decomposed one has a list of binary labels  $L_i$ , using the label assignment

Scenes	Single View		MVSeg		SA3D		Ours	
	IoU	Acc	IoU	Acc	IoU	Acc	IoU	Acc
Orchids	79.4	96.0	92.7	98.8	83.6	96.9	85.4	97.5
Ferns	95.2	99.3	94.3	99.2	97.1	99.6	92.0	98.9
Room	73.4	96.5	95.6	99.4	88.2	98.3	86.5	98.1
Horns	85.3	97.1	92.8	98.7	94.5	99.0	91.1	98.4
Fortress	94.1	99.1	97.7	99.7	98.3	99.8	96.6	99.5
Fork	69.4	98.5	87.9	99.5	89.4	99.6	83.4	99.3
Pinecone	57.0	92.5	93.4	99.2	92.9	99.1	92.0	99.0
Truck	37.9	77.9	85.2	95.1	90.8	96.7	93.0	97.9
Lego	76.0	99.1	74.9	99.2	92.2	99.8	88.4	99.7
Mean	74.1	95.2	90.5	98.8	91.9	98.8	89.9	98.7

Table 1. Quantitative results on SPIIn-NeRF dataset

in Sec. 3.3. Leveraging the assigned labels, here we adopt a simple yet effective heuristic rule to determine if a 3D Gaussian  $g_i$  belongs to the target 3D object. In particular, we first define the confidence score  $s_i$  of  $g_i$  as

$$s_i = \frac{1}{N} \sum_{j=0}^{N-1} L_{ij}, \quad (9)$$

where  $N$  is the number of views. Then we adopt a threshold  $\tau$  and regard a Gaussian with a score higher than  $\tau$  as positive.

## 4. Experiments

### 4.1. Datasets

We choose different datasets to testify our method, including LLFF [19], Mip-NeRF 360 [2], LERF [12], and some test scenes from the 3D Gaussian Splatting [11]. These datasets contain both small indoor objects and large outdoor scenes, which are very complex and challenging. For quantitative experiments, because there is no existing benchmark that can be used in 3D Gaussian space, we use the SPIIn-NeRF [21] dataset with 2D ground-truth for evaluation.

### 4.2. Quantitative results

We first conduct experiments on the SPIIn-NeRF [21] dataset for quantitative analysis. Given a set of images of the scene, we follow the process described in Section 3 to obtain the segmentation of the target object in 3D Gaussian Space. The segmented 3D Gaussians are used to render 2D masks in other views. Finally, we calculate the IoU and Accuracy between these rendered and the ground-truth masks. Results can be seen in Table 1.

In the comparison, it is noteworthy that both the MVSeg [21] and the SA3D [3] require additional parameters and a computation-costly training process. By contrast, the “Single view” [3] refers to mapping the 2D masks

Scene	room	truck	fortress	pinecone
Text	“the table”	“the truck”	“the fortress”	“the pinecone”
IoU	86.3	93.7	92.8	86.5
Acc	97.9	97.8	98.8	97.0

Table 2. Quantitative results with text prompts on four scenes of SPIIn-NeRF dataset.

to the 3D space based on the corresponding depth information, which does not need additional training process. In this sense, our method is the same as the “Single view” that does not incorporate any additional training or model parameters. Results show that our approach can achieve comparable segmentation quality to the learnable MVSeg and SA3D methods. In some 360 outdoor scenes, such as “Truck”, our approach even outperforms the SA3D and the MVSeg. When compared with the training-free method “Single view”, our approach achieves a significant promotion of +15.8% IoU and +3.5% Acc. These results demonstrate our approach is very efficient in obtaining high-quality segmentation masks.

Next, we replace the above point prompts with text prompts corresponding to the objects. Given a text input, we prompt the Grounding DINO [16] to generate target bounding boxes, which serve as input prompts for the SAM to obtain 2D segmentation masks. Then, following the segmentation process in Section 3, we can transform the 2D masks into 3D Gaussian masks corresponding to the text input. Similar to the above evaluation process, we also calculate the IoU and Acc between 2D rendered masks and given ground-truth masks. Quantitative results are shown in Table 2. For both room and truck scenes, the IoU and Acc values can achieve a similar level as using clicked points as input prompts. These results demonstrate our method has the ability to combine multi-modal prompts as input.

### 4.3. Qualitative results

We conduct four kinds of tasks to demonstrate the potential application and qualitative performance of our approach, including point-guided segmentation, text-guided segmentation, scene editing, and collision detection.

**Point-Guided Segmentation:** We first conduct visualization experiments on 3D object segmentation guided by one or a set of point prompts clicked on the first-view rendered image. The results are shown in Figure 4. Our approach demonstrates stable performance in diverse scenes and target objects, including multiple instance segmentation (1st row), salient object segmentation (2nd row), and partial segmentation (3rd row). Even when the target objects are of extremely small scales (the first row), our approach can still produce high-quality segmentation.



Figure 4. Visualization of segmentation results in different scenes (LERF-figurines [12], LERF-dozer-nerfgun-waldo [12], SPIn-NeRF-Orchids [21]). We enlarge the boxed area on the right for a better visualization.

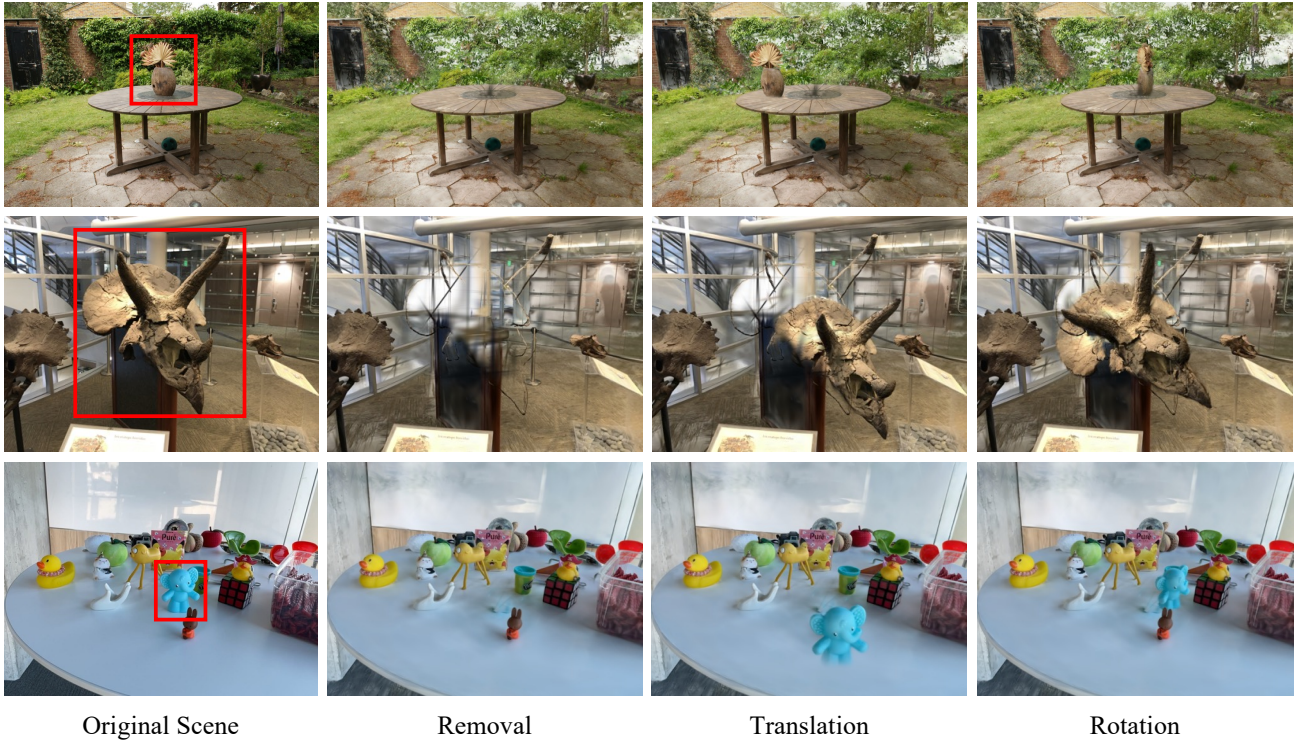


Figure 5. Visualization examples of scene editing after the object segmentation. We offer three scene editing examples: removal, translation, and rotation.

Scene	w/ GD		w/o GD		Delete	
	IoU	Acc	IoU	Acc	IoU	Acc
Orchids	85.4	97.5	82.2	96.8	78.2	95.4
Ferns	92.0	98.9	89.2	98.4	89.8	98.5
Room	86.5	98.1	81.3	97.2	85.4	97.9
Horns	91.1	98.4	83.2	96.5	84.8	97.6
Fortress	96.5	99.4	88.5	98.1	82.3	96.7
Fork	83.4	99.3	81.8	99.2	79.9	99.1
Pinecone	92.1	98.9	91.6	98.9	82.9	97.5
Truck	94.0	97.9	93.4	97.8	91.4	96.8
Lego	88.4	99.7	88.4	99.6	82.9	99.4
mean	<b>89.9</b>	98.7	86.6	98.1	84.2	97.7

Table 3. Ablation on Gaussian decomposition (GD) on SPIn-NeRF dataset. The 2nd and 3rd columns compare the results before and after using the Gaussian decomposition (GD). The last column represents the results of directly removing the gaussians across mask boundaries.



Figure 6. 3D segmentation results with text prompts in Mip-NeRF360-garden [2].

**Text-Guided Segmentation:** Next, we further conduct 3D object segmentation experiments guided by text prompts. We follow the same process as in Table 2 experiments to conduct visualization experiments. In order to compare our method with SA3D under the same setting, we choose the same garden scene from Mip-NeRF 360 dataset [2], using three text prompts including “The table”, “The vase” and “The bonsai”. Results in Figure 6 show that our approach can achieve accurate segmentation results by simply providing object names, which demonstrates the potential of our method in combining with language models. Compared with the SA3D in the “The table” case, our approach can segment the complete object with desired table legs, while SA3D only gives the tabletop.

**Scene Editing:** Scene editing is a basic application for 3D reconstructed scenes. However, it’s quite difficult to do this without being able to locate the specific objects. This task demonstrates the ability of our approach to help edit the 3D scenes. Specifically, after segmenting the objects in the 3D

Number of views	5(10%)	10(20%)	21(50%)	42(100%)
IoU on Fortress	91.16	92.11	93.82	96.55
Number of views	25(10%)	50(20%)	125(50%)	251(100%)
IoU on truck	90.27	90.97	92.11	93.48

Table 4. Ablation on different number of views for 3D segmentation. Numbers in parentheses represent the used view percentage of the total training view.

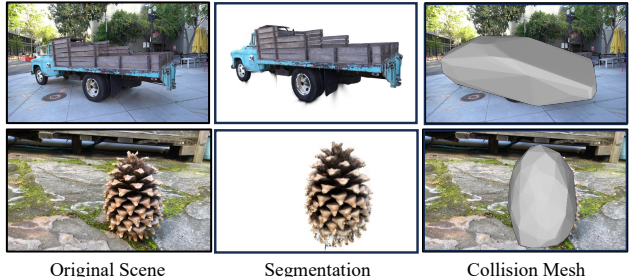


Figure 7. Collision mesh for segmented 3D objects using QuickHull algorithm.

$\tau$	0.3	0.5	0.6	0.7	0.9
IoU	61.7	82.7	<b>93.4</b>	90.6	53.9

Table 5. Ablation on confidence score threshold  $\tau$  on the “truck” scene.

Gaussian space, we can manipulate the objects by removing, translating, and rotating them. Thanks to the simplicity of the explicit Gaussian representations, without bells and whistles, our approach obtains satisfactory scene editing results, as shown in Figure 5. The instances in 1st column with red bounding boxes are objects to be segmented. It can be seen that with objects segmented in 3D Gaussians, they can be translated and rotated in any direction in the scene. After the removal of segmented objects, original scenes can still keep intact.

**Collision Detection:** Collision detection is an indispensable component in practical 3D applications, such as games, movies, and simulators. In this task, we demonstrate our approach can directly help in revealing the collision body of target objects in the 3D Gaussian space. We choose two scenes from SPIn-NeRF dataset. Following the process of our segmentation method, we can obtain the corresponding segmented 3D Gaussian points in the scene. To this end, we use the Quickhull [1] algorithm to build the collision mesh upon our segmented objects. The results in Figure 7 show that our segmented objects can successfully derive correct convex hulls for downstream applications.

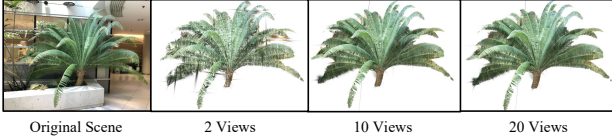


Figure 8. The influence of different view numbers on LERF-fern.

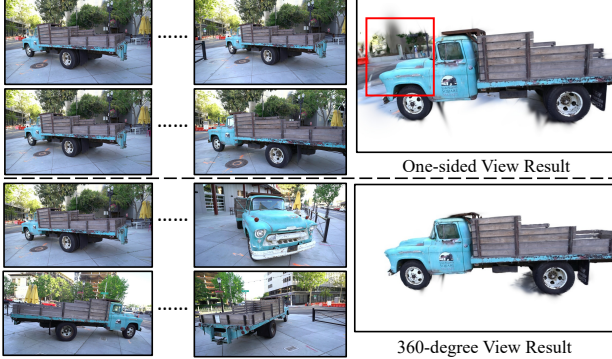


Figure 9. The influence of different view directions.

#### 4.4. Ablation Study

**Selection of Views:** In this section, we study the influence of selected 2D views on 3D Gaussian segmentation. Figure 8 demonstrates the segmentation quality using different numbers of views. It is noteworthy that the leaves in the “fern” scene are very tiny and challenging. Even so, with only two sparse views, our approach can achieve decent results, and the segmentation quality quickly improves when increasing the number of views. Table 4 also draws a similar conclusion: as the number of views increases, the IoU values will also increase. It is worth noting that even with sparse views (10% percentage), we can obtain relatively decent results for both two types of scenes, which also demonstrates the robustness and effectiveness of our approach. In practical applications, using sparse views (below 10% of total views) will greatly improve efficiency, although under 100% views, our method can still be completed within one minute.

Figure 9 studies the influence of view directions on final segmentation results. We choose the truck with 360-degree views. The upper row shows the result of using roughly a single direction. In this case, the background is mistakenly incorporated into the segmentation. By contrast, with the same number of views but variant directions, the approach achieves high-quality clean segmentation results. This result reveals the importance of choosing non-monotone view directions in practice usage with 360 scenes.

**Gaussian Decomposition:** Gaussian Decomposition is proposed to address the issue of roughness boundaries of 3D segmented objects, which results from the non-negligible spatial sizes of 3D Gaussian located at the boundary. We conduct both quantitative and qualitative experiments to verify the effectiveness of our approach. For quantitative

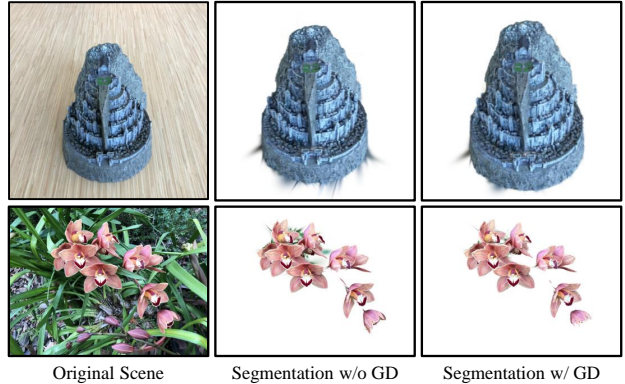


Figure 10. Ablation results on Gaussian Decomposition (GD) on the LERF-pinecone.

ablation experiments, Table 3 shows the results. We compare our proposed Gaussian Decomposition scheme with two other processing methods, one for segmentation without any special handling (the 3rd column), and the other for directly removing such gaussians (the last column). The experiments are conducted on SPIIn-NeRF dataset, following the same evaluation process as Table 1. Compared with the others, our proposed approach outperforms them on all scenes with +3.3% and +5.7% IoU, respectively, demonstrating the effectiveness of Gaussian Decomposition. Besides, it can be seen that directly removing these gaussians cannot decrease the roughness of mask boundaries, leading to even 2.4% lower IoU values.

Figure 10 shows the visualization results for comparison. We select two representative scenes in which the junction/contact exists large-scale Gaussian points (can be seen in the 2nd column). This issue is alleviated after utilizing the proposed Gaussian Decomposition strategy. Though this idea is simple, the improvement is obvious.

**Hyper-Parameters:** In the process of our method, we set a hyper-parameter  $\tau$  to control the threshold of label confidence score in Section 3.5. As shown in Table 5, too large  $\tau$  values will lead to the partially missing the segmented objects, and too small  $\tau$  values will remain more background objects. For scenes with some views that may cover only part of the objects to be segmented (i.e. half of the truck body in the “truck” scene), a small  $\tau$  value is preferred. In the interactive segmentation process, this threshold can be set manually according to the complexity of the scenes and the quality of camera views.

## 5. Conclusion

In this paper, we present a novel approach for object segmentation in 3D Gaussians, which performs an interactive procedure without any training process and learnable parameters. Based on a trained 3D Gaussian representation and clicked points on first view, we propose the multiview

mask generation and view-wise label assignment scheme to generalize SAM to achieve 3D segmentation. In addition, we provide the Gaussian Decomposition to mitigate the boundary roughness issue of segmented masks, and the cross-view label voting approach to assign labels from different views. Extensive segmentation experiments show that our method can effectively obtain high-quality object segmentation results in 3D Gaussians, which can be easily applied for scene editing and collision detection tasks. Overall, we hope our work can inspire more future work in the area of 3D Gaussian representation.

## References

- [1] C Bradford Barber, David P Dobkin, and Hannu Huhdanpaa. The quickhull algorithm for convex hulls. *ACM Transactions on Mathematical Software (TOMS)*, 22(4):469–483, 1996. 7
- [2] Jonathan T Barron, Ben Mildenhall, Dor Verbin, Pratul P Srinivasan, and Peter Hedman. Mip-nerf 360: Unbounded anti-aliased neural radiance fields. In *Proceedings of the IEEE/CVF Conference on Computer Vision and Pattern Recognition*, pages 5470–5479, 2022. 5, 7
- [3] Jiazhong Cen, Zanwei Zhou, Jiemin Fang, Wei Shen, Lingxi Xie, Xiaopeng Zhang, and Qi Tian. Segment anything in 3d with nerfs. *arXiv preprint arXiv:2304.12308*, 2023. 1, 2, 5
- [4] Anpei Chen, Zexiang Xu, Andreas Geiger, Jingyi Yu, and Hao Su. Tensorf: Tensorial radiance fields. In *Proc. ECCV*, pages 333–350. Springer, 2022. 1
- [5] Zilong Chen, Feng Wang, and Huaping Liu. Text-to-3d using gaussian splatting. *arXiv preprint arXiv:2309.16585*, 2023. 2
- [6] Lue Fan, Xuan Xiong, Feng Wang, Naiyan Wang, and Zhaoxiang Zhang. Rangedet: In defense of range view for lidar-based 3d object detection. In *Proc. ICCV*, pages 2918–2927, 2021. 1
- [7] Lue Fan, Feng Wang, Naiyan Wang, and ZHAO-XIANG ZHANG. Fully sparse 3d object detection. *Advances in Neural Information Processing Systems*, 35:351–363, 2022. 1
- [8] Rahul Goel, Dhawal Sirikonda, Saurabh Saini, and PJ Narayanan. Interactive segmentation of radiance fields. In *Proceedings of the IEEE/CVF Conference on Computer Vision and Pattern Recognition*, pages 4201–4211, 2023. 2
- [9] Qingyong Hu, Bo Yang, Sheikh Khalid, Wen Xiao, Niki Trigoni, and Andrew Markham. Towards semantic segmentation of urban-scale 3d point clouds: A dataset, benchmarks and challenges. In *Proc. CVPR*, pages 4977–4987, 2021. 1
- [10] Haian Jin, Isabella Liu, Peijia Xu, Xiaoshuai Zhang, Songfang Han, Sai Bi, Xiaowei Zhou, Zexiang Xu, and Hao Su. Tensoir: Tensorial inverse rendering. In *Proc. CVPR*, pages 165–174, 2023. 1
- [11] Bernhard Kerbl, Georgios Kopanas, Thomas Leimkühler, and George Drettakis. 3d gaussian splatting for real-time radiance field rendering. *ACM Transactions on Graphics*, 42(4):1–14, 2023. 1, 2, 3, 5
- [12] Justin Kerr, Chung Min Kim, Ken Goldberg, Angjoo Kanazawa, and Matthew Tancik. Lerf: Language embedded radiance fields. In *Proceedings of the IEEE/CVF International Conference on Computer Vision*, pages 19729–19739, 2023. 2, 5, 6
- [13] Alexander Kirillov, Eric Mintun, Nikhila Ravi, Hanzi Mao, Chloe Rolland, Laura Gustafson, Tete Xiao, Spencer Whitehead, Alexander C Berg, Wan-Yen Lo, et al. Segment anything. *arXiv preprint arXiv:2304.02643*, 2023. 1, 2
- [14] Xin Lai, Jianhui Liu, Li Jiang, Liwei Wang, Hengshuang Zhao, Shu Liu, Xiaojuan Qi, and Jiaya Jia. Stratified transformer for 3d point cloud segmentation. In *Proc. CVPR*, pages 8500–8509, 2022. 1
- [15] Zhiqi Li, Wenhui Wang, Hongyang Li, Enze Xie, Chonghao Sima, Tong Lu, Yu Qiao, and Jifeng Dai. Bevformer: Learning bird’s-eye-view representation from multi-camera images via spatiotemporal transformers. In *Proc. ECCV*, pages 1–18. Springer, 2022. 1
- [16] Shilong Liu, Zhaoyang Zeng, Tianhe Ren, Feng Li, Hao Zhang, Jie Yang, Chunyuan Li, Jianwei Yang, Hang Su, Jun Zhu, et al. Grounding dino: Marrying dino with grounded pre-training for open-set object detection. *arXiv preprint arXiv:2303.05499*, 2023. 5
- [17] Jonathon Luiten, Georgios Kopanas, Bastian Leibe, and Deva Ramanan. Dynamic 3d gaussians: Tracking by persistent dynamic view synthesis. *arXiv preprint arXiv:2308.09713*, 2023. 2
- [18] Gregory P Meyer, Ankit Laddha, Eric Kee, Carlos Vallespi-Gonzalez, and Carl K Wellington. Lasernet: An efficient probabilistic 3d object detector for autonomous driving. In *Proc. CVPR*, pages 12677–12686, 2019. 1
- [19] Ben Mildenhall, Pratul P Srinivasan, Rodrigo Ortiz-Cayon, Nima Khademi Kalantari, Ravi Ramamoorthi, Ren Ng, and Abhishek Kar. Local light field fusion: Practical view synthesis with prescriptive sampling guidelines. *ACM Transactions on Graphics (TOG)*, 38(4):1–14, 2019. 5
- [20] B Mildenhall, PP Srinivasan, M Tancik, JT Barron, R Ramamoorthi, and R Ng. Nerf: Representing scenes as neural radiance fields for view synthesis. In *Proc. ECCV*, 2020. 1
- [21] Ashkan Mirzaei, Tristan Amentado-Armstrong, Konstantinos G Derpanis, Jonathan Kelly, Marcus A Brubaker, Igor Gilitschenski, and Alex Levinshtein. Spin-nerf: Multiview segmentation and perceptual inpainting with neural radiance fields. In *Proceedings of the IEEE/CVF Conference on Computer Vision and Pattern Recognition*, pages 20669–20679, 2023. 5, 6
- [22] Mong H Ng, Kaahan Radia, Jianfei Chen, Dequan Wang, Ionel Gog, and Joseph E Gonzalez. Bev-seg: Bird’s eye view semantic segmentation using geometry and semantic point cloud. *arXiv preprint arXiv:2006.11436*, 2020. 1
- [23] Cong Pan, Yonghao He, Junran Peng, Qian Zhang, Wei Sui, and Zhaoxiang Zhang. Baeformer: Bi-directional and early interaction transformers for bird’s eye view semantic segmentation. In *Proc. CVPR*, pages 9590–9599, 2023. 1
- [24] Xuran Pan, Zhuofan Xia, Shiji Song, Li Erran Li, and Gao Huang. 3d object detection with pointformer. In *Proc. CVPR*, pages 7463–7472, 2021. 1
- [25] Lang Peng, Zhirong Chen, Zhangjie Fu, Pengpeng Liang, and Erkang Cheng. Bevsegformer: Bird’s eye view semantic

- segmentation from arbitrary camera rigs. In *Proc. WACV*, pages 5935–5943, 2023. 1
- [26] Zhongzheng Ren, Aseem Agarwala, Bryan Russell, Alexander G Schwing, and Oliver Wang. Neural volumetric object selection. In *Proceedings of the IEEE/CVF Conference on Computer Vision and Pattern Recognition*, pages 6133–6142, 2022. 2
- [27] Shaoshuai Shi, Xiaogang Wang, and Hongsheng Li. Pointrcnn: 3d object proposal generation and detection from point cloud. In *Proc. CVPR*, pages 770–779, 2019. 1
- [28] Cheng Sun, Min Sun, and Hwann-Tzong Chen. Direct voxel grid optimization: Super-fast convergence for radiance fields reconstruction. In *Proc. CVPR*, pages 5459–5469, 2022. 1
- [29] Jiaxiang Tang, Jiawei Ren, Hang Zhou, Ziwei Liu, and Gang Zeng. Dreamgaussian: Generative gaussian splatting for efficient 3d content creation. *arXiv preprint arXiv:2309.16653*, 2023. 2
- [30] Vadim Tschernezki, Iro Laina, Diane Larlus, and Andrea Vedaldi. Neural feature fusion fields: 3d distillation of self-supervised 2d image representations. In *2022 International Conference on 3D Vision (3DV)*, pages 443–453. IEEE, 2022. 2
- [31] Chenyu Yang, Yuntao Chen, Hao Tian, Chenxin Tao, Xizhou Zhu, Zhaoxiang Zhang, Gao Huang, Hongyang Li, Yu Qiao, Lewei Lu, et al. Bevformer v2: Adapting modern image backbones to bird’s-eye-view recognition via perspective supervision. In *Proc. CVPR*, pages 17830–17839, 2023. 1
- [32] Taoran Yi, Jiemin Fang, Guanjun Wu, Lingxi Xie, Xiaopeng Zhang, Wenyu Liu, Qi Tian, and Xinggang Wang. Gaussian-dreamer: Fast generation from text to 3d gaussian splatting with point cloud priors. *arXiv preprint arXiv:2310.08529*, 2023. 2
- [33] Shuaifeng Zhi, Tristan Laidlow, Stefan Leutenegger, and Andrew J Davison. In-place scene labelling and understanding with implicit scene representation. In *Proceedings of the IEEE/CVF International Conference on Computer Vision*, pages 15838–15847, 2021. 2
- [34] Matthias Zwicker, Hanspeter Pfister, Jeroen Van Baar, and Markus Gross. Ewa volume splatting. In *Proceedings Visualization, 2001. VIS’01.*, pages 29–538. IEEE, 2001. 4

# Segment Anything in 3D Gaussians

## Supplementary Material

### 1. Implementation Details

As the implementation of 3D Gaussian Splatting for each scene, we follow the official code with default parameters, and each scene is trained with 30000 iterations. For the first view 2D mask, we don't limit the number of points for SAM. This is reasonable since users can refine their input prompts to help SAM generate a 2D mask as accurately as possible from the reference view. For the selection of hyper-parameters, we only have one to control, which is the confidence score threshold  $\tau$  in the Multiview Label Voting method. We have already done related ablation studies. According to our ablation results, we set the value in the range of 0.6 to 0.8 to obtain better results in most experiments. Also, in practical use, users can manually set this value according to the complexity of different scenes. As for the number of views used in experiments, we follow SA3D to select all view images of each scene to finish our segmentation process. However, in practice, this value can be decreased according to our ablation.

### 2. More Visualization Results

**Collision Results** After obtaining the 3D segmentation of the object, we can directly use the existing algorithm to calculate its collision mesh, and then perform collision detection. We provide a video of collision detection (see “collision.mp4”).

The scene in the video is a real-time rendered 3D GS (3D Gaussian Splatting) scene. We first perform 3D segmentation on the object truck following our pipeline and then calculate its corresponding collision mesh for collision. Afterward, we throw balls at the truck to show collision responses. It can be observed that balls will be bounced off after touching the truck body, instead of going straight through it. Video ”no\_collision.mp4“ shows the same scene but without adding any collision, where the balls directly pass through the truck. This proves that after using our method to obtain 3D Gaussian Segmentation, it is very convenient to add collision to the objects in the 3D GS, realizing collision responses.

**Text-guided Visualization Results** We present more segmentation results with text prompts as input, as shown in Figure 1. The first scene is of 360-degree views, while the other two are forward-facing scenes. We follow the same process: first, prompt the Grounding DINO to generate target bounding boxes with given texts, which serve as input prompts for the SAM to obtain 2D segmentation masks;

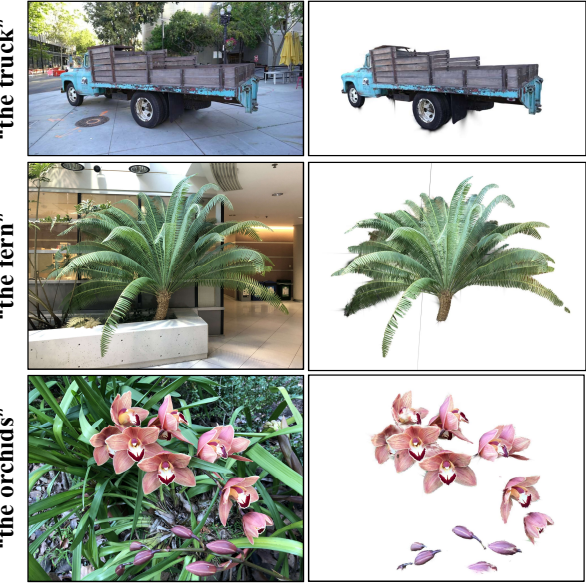


Figure 1. More text-guided segmentation results.

Then, following our segmentation method, we can transform the 2D masks into 3D Gaussian masks corresponding to the text input. More visualization results showcase the effectiveness of our method across various input prompts.

**More Segmentation Results** We present more visualization results in Figure 2, showing the effectiveness of our method. Guided by one or a set of point prompts clicked on the first-view rendered image, our method can achieve high-quality segmentation results.

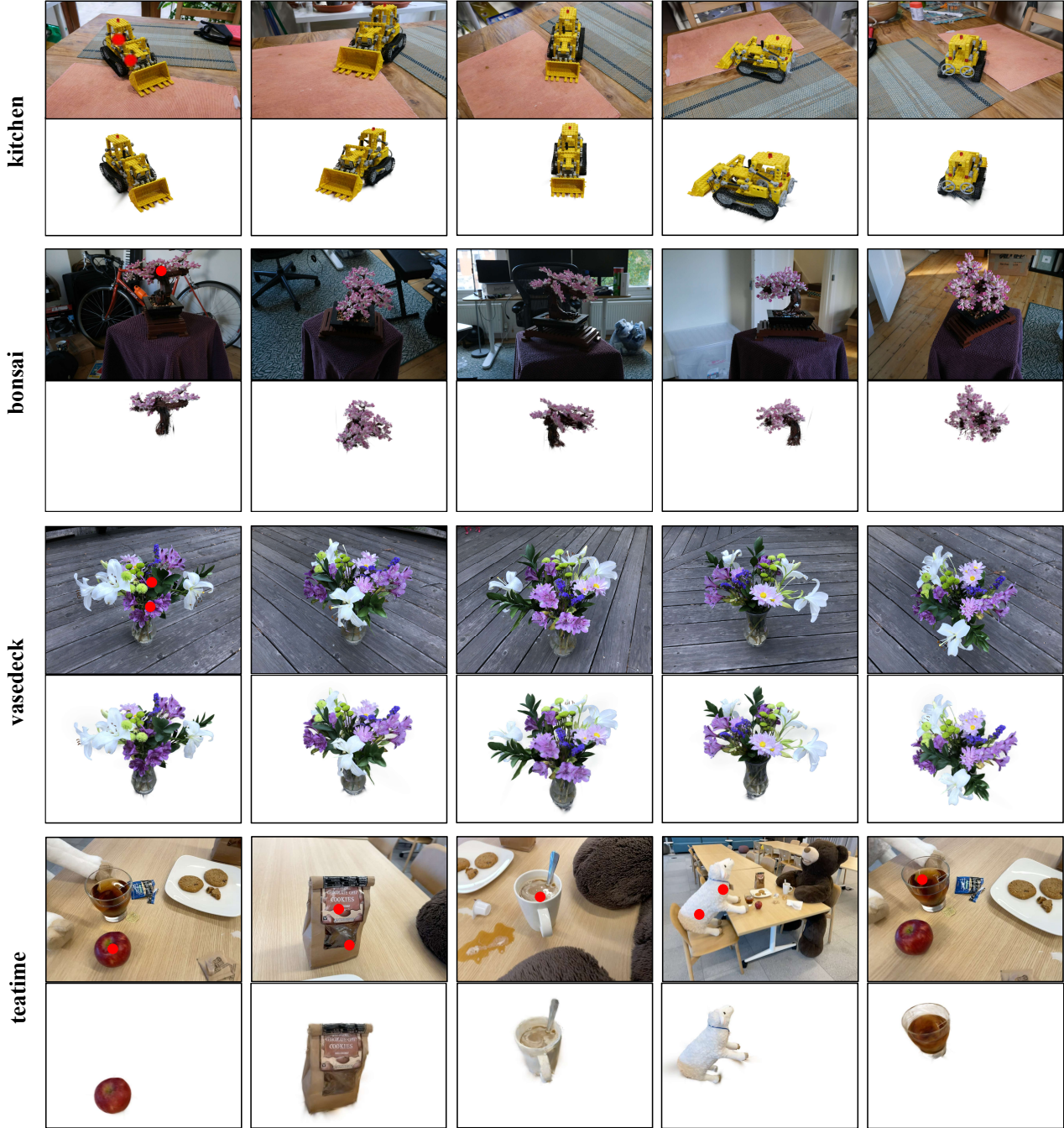


Figure 2. More visualization segmentation results.